Mesoscopic Simulation on Phase Behavior of Ternary Copolymeric Solution in the Absence and Presence of Shear

Xiuqing Zhang,† Shiling Yuan,*,†,‡ and Jian Wu‡

Key Laboratory of Colloid and Interface Chemistry, Shandong University, Jinan 250100, China, and Institute of Theoretical Chemistry, Shandong University, Jinan 250100, China

Received May 29, 2006; Revised Manuscript Received July 11, 2006

ABSTRACT: We simulate the microphase separation dynamics of the triblock polymer surfactant (ethylene oxide)$_{19}$(propylene oxide)$_{29}$(ethylene oxide)$_{19}$ (P65) in aqueous solution by a dynamic variant of mean-field density functional theory for Gaussian chains. With the increase of concentration, different mesoscale structures are found in the absence and presence of shear. (1) In the absence of shear, there are three morphologies formed. The first is the micellar phase, including a spherical micelle, which has hexagonal packing and a fcc (face-centered cubic) structure in the solution and a wormlike micelle, the second is the bicontinuous phase, which belongs to gyroid-type connectivity, and the third is the lamellar phase. (2) In the presence of shear, only two morphologies are formed in all concentrations, they are hexagonal and lamellar phases, which align in the flow direction. We notice that the weak shear makes the order parameters of the simulation system oscillate, while the strong shear makes the order parameter get equilibrated in a short time. It is concluded that the mesoscopic simulation method is a valuable tool for description of mesoscale morphology formation in the absence or presence of shear and can give mesoscale information for the experiments.

1. Introduction

Pluronics, also termed poloxamers or synperonics, are block PEO−PPO−PEO copolymers of poly(ethylene oxide) (PEO) and poly(propylene oxide) (PPO). In aqueous solution, these block copolymers behave like surfactant molecules and build a wide variety of aggregates as a consequence of their amphiphilic character. Under appropriate conditions, they form multimolecular micellar, bicontinuous, hexagonal, and lamellar phases. The properties of Pluronics aggregates have been extensively investigated via many techniques such as microcalorimetry,[1−3] small-angle neutron or X-rays scattering,[4−7] static[8] and dynamic[9,10] light scattering, or rheometry.[11−14] In these studies, the spherical micelles are typical, in which a hydrophobic block is gathered into a spherical core and the hydrophilic blocks are solvated by water. These experimental investigations about different aggregates are helpful to understand the structures and properties of Pluronic solution.

In the past decade, computer simulation methods have been proven to be valuable tools to study the phase behavior of polymers. All-atomic molecular dynamics (MD) simulation approaches would permit modeling of morphological evolution in polymeric systems during phase separation. Furthermore, the mesoscopic simulation method is another useful simulation approach that has been widely accepted, such as dissipative particle dynamics (DPD)[15−18] and mesoscopic dynamics (MesoDyn).[19−21] And these mesoscopic models form a bridge between fast molecular kinetics and slow thermodynamic relaxation of macroscale properties.[22] They treat the polymeric chains in a coarse-grained (or mesoscopic) level by grouping atoms together up to the persistence length of polymer chains, which could be extended to several orders of magnitude in length and time scales compared to all-atomic MD simulations.[23] Essentially as an MD simulation procedure, DPD is similar to Brownian dynamics, wherein particles are subjected to conservative, dissipative, and random forces that are calculated for pairs of neighboring particles. The method employs the soft interaction potentials, allowing large time-scale simulations, and time evolution of the system is found by solving Newton's equations of motion.[23] MesoDyn simulation is based on dynamic mean-field density functional theory, and it has led to significant advances in the investigation of the microphase separation of block copolymers.[24−27] An important advantage of MesoDyn is the time integration of functional Langevin equations. Potential applications of MesoDyn include the simulation of the time evolution of micelle formation, drug delivery, phase behavior of block copolymers, formation of mesoscale structures, the solution behavior of specific chemical species, etc.[25−27]

In contrast with previous approaches aimed at classifying morphologies by means of equilibrium theories, the Mesodyn method recognizes the fact that these patterns are irregular in nature, and they can only be characterized via the dynamic properties of the systems. This approach is much more realistic from an industrial perspective. Furthermore, its typical processing times are orders of magnitude, which is shorter than the thermodynamic relaxation time, and thus such irregular states contribute substantially to the behavior of the final materials.[28] Another important advantage of this method is that there is no a prior assumption on the phases, so the kinetics of phase formation, which is very difficult to observe in the experiment, can be studied.

In this present study, MesoDyn simulation has been performed for Pluronics, (ethylene oxide)$_{19}$(propylene oxide)$_{29}$-(ethylene oxide)$_{19}$ (P65), in aqueous solution. We simulate the morphology formation by an instantaneous quench from homogeneous density distribution. The evolution of the mesoscale structures is followed directly from observation of 3D density fields, and the time scale of phase separation is on the order of milliseconds−seconds. The mesoscale structure and different-phase regions are shown in the absence and presence of shear. According to our simulations, the polymer P65 forms three

* To whom correspondence should be addressed. E-mail: shilingyuan@sdu.edu.cn. Telephone: +86 531 88366031. Fax: +86 531 88564464.

† Key Laboratory of Colloid and Interface Chemistry.

‡ Institute of Theoretical Chemistry.

10.1021/ma061201b CCC: $33.50
Published on Web 08/18/2006

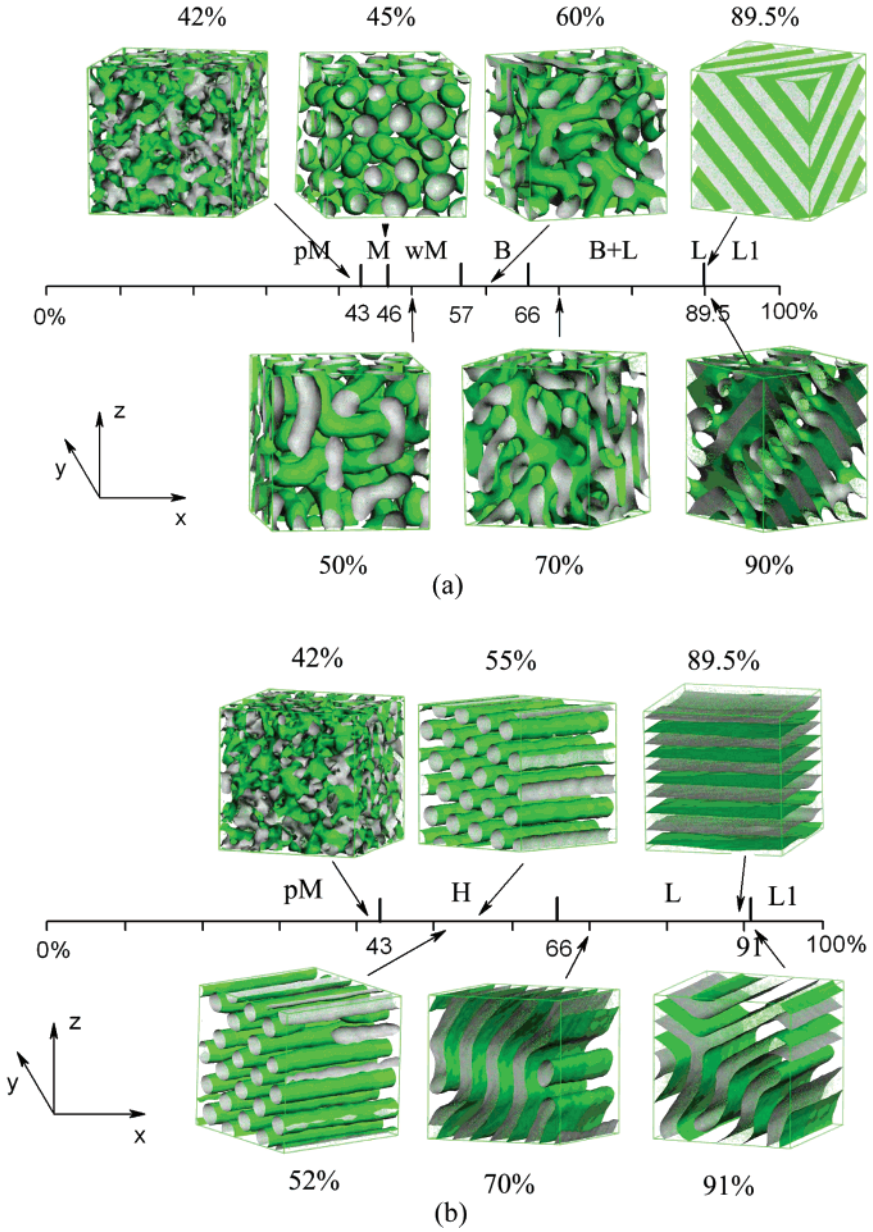

Figure 1. Simulated phase diagram of Pluronic solution at 298 K. The concentrations are in polymer vol %. The observed microphases are shown at the top of each diagram. pM, M, wM, B, L, L1, and H denote premicellar, micellar, wormlike micellar, bicontinuous, lamellar, defected lamellar, and hexagonal phase, respectively. (a) Phases in the absence of shear; (b) phases in the presence of shear ($\dot{\gamma} = 5 \times 10^5\ s^{-1}$).

different phases (micellar, bicontinuous, and lamellar) in a big 43−89.5 vol % concentration interval in the absence of shear, and two different phases (hexagonal and lamellar) in the similar concentration interval in the presence of shear (in Figure 1). In contrast with the morphology of solution in the absence of shear, the micellar-phase and bicontinuous-phase regions disappear in the presence of shear, and one new phase region, the hexagonal-phase, appears and the lamellar-phase region is extended (in Figure 1b).

The paper is arranged as follows: we first elaborate on the approaches to the transition Gaussian chain and the interaction parameters which are used in MesoDyn, and the background of the method is simply introduced; then, different morphologies are shown and investigated using the 3D density fields in the absence and presence of shear.

2. Simulation Method and Details

2.1. Theory in MesoDyn. The MesoDyn simulation is basic on the dynamics density functional theory (DDFT). The basic idea of this method is that if the free energy F of an inhomogeneous liquid is a function of the local density function ρ, then all thermodynamic functions can be derived.[24−28]

The model used in the MesoDyn project consists of beads of various types, I, J, ..., with interactions described by harmonic oscillator potentials for the intramolecular interactions (Gaussian chain) and a mean-field potential for all other interactions.[29] Each bead is a certain component type representing covalently bonded groups of atoms such as those given by one or a few structural units of a polymer chain. The dynamics of system is described by a set of functional Langevin equations, and these equations are the diffusion equations in the component densities, which take account of the noise in the system.

On a coarse-grained time scale, $\rho_I^0(\mathbf{r})$ is defined as a collective concentration field of the type I beads at an instant of time and serves as a reference level. There will be a certain distribution of bead positions, defined as $\psi(\mathbf{R}_{11}, ..., \mathbf{R}_{nN})$, where $\mathbf{R}_{\lambda s}$ is the position of bead s from chain λ. Given the distribution ψ, the collective concentration of bead s from all chains can be defined

by the average of a microscopic density operator:

$$\rho_I[\psi](\mathbf{r}) \equiv \sum_{r=1}^{n}\sum_{s=1}^{N}\delta_{Is}^{K}\mathrm{Tr}\psi\delta(\mathbf{r}-\mathbf{R}_{\lambda s}) \quad (1)$$

(δ_{Is}^{K} is the Kronecker function with value 1 when bead s is of type I and 0 otherwise). It is assumed that the interactions do not depend on the momenta in a liquid with high viscosity (slowly relaxation). A set of distribution functions ψ is defined with the constraint $\rho_I^0(\mathbf{r}) = \rho_I[\psi](\mathbf{r})$. All distributions ψ belong to the same density $\rho_I^0(\mathbf{r})$ from an equivalence class Ω of distribution functions:

$$\Omega = \{\psi(\mathbf{R}_{11}, ..., \mathbf{R}_{nN})|\rho_I[\psi](\mathbf{r}) = \rho_I^{\ 0}(\mathbf{r})\} \quad (2)$$

On the basis of this set of distribution functions, an intrinsic free-energy functional $F[\psi]$ can be defined:

$$F[\psi] = \mathrm{Tr}(\psi H^{id} + \beta^{-1}\psi \ln \psi) + F^{nid}[\rho^0] \quad (3)$$

The first term is the average value of the Hamiltonian for the internal Gaussian chain.[24] The second term in the free-energy functional represents the entropy of the distribution $-k_BT\psi \ln \psi$. The third term is the mean-field nonideal contribution. ψ is independent of the history of system and is fully characterized by the constraint (on the density distribution that minimizes the free-energy function). This constraint is realized by means of an external potential U_I.

The constraint minimization of the free-energy functional leads to an optimal distribution, which can be written in terms of densities and external potential as:

$$F[\rho] = -\beta^{-1}n \ln \Phi + \beta^{-1}\ln n! - \sum_I \int U_I(\mathbf{r})\rho_I(\mathbf{r})\,d\mathbf{r} + F^{nid}[\rho] \quad (4)$$

Φ is the partition function of the chain. Now, the model for the nonideal free-energy functional is introduced,

$$F^{nid}[\rho] = \frac{1}{2}\int\int\begin{bmatrix}\epsilon_{AA}(|\mathbf{r}-\mathbf{r}'|)\rho_A(\mathbf{r})\rho_A(\mathbf{r}') + \epsilon_{AB}(|\mathbf{r}-\mathbf{r}'|)\rho_A(\mathbf{r})\rho_B(\mathbf{r}') \\ +\epsilon_{BA}(|\mathbf{r}-\mathbf{r}'|)\rho_B(\mathbf{r})\rho_A(\mathbf{r}') + \epsilon_{BB}(|\mathbf{r}-\mathbf{r}'|)\rho_B(\mathbf{r})\rho_B(\mathbf{r}')\end{bmatrix}d\mathbf{r}d\mathbf{r}' \quad (5)$$

where $\epsilon_{IJ}(|\mathbf{r}-\mathbf{r}'|)$ is a mean-field energetic interaction between beads of type I at $\mathbf{r}$ and type J at $\mathbf{r}'$.

The mean-field intrinsic chemical potentials can easily be derived via functional differentiation of the free energy: $\mu_I(\mathbf{r}) = \delta F/\delta\rho_I(\mathbf{r})$. At equilibrium, $\mu_I(\mathbf{r}) =$ constant, which results in the familiar self-consistent-field equations for the mean-field Gaussian chain model. In general, these equations have many solutions, corresponding to stable or metastable states, and the one with the lowest free energy is of particular interest. On the basis of these equations, the generalized time-dependent Ginzburg−Landau theory can be set up[24]

$$\frac{\partial\rho_A(\mathbf{r})}{\partial t} = Mv\nabla\cdot\rho_A\rho_B\nabla[\mu_A - \mu_B] + \eta \quad (6)$$

$$\frac{\partial\rho_B(\mathbf{r})}{\partial t} = Mv\nabla\cdot\rho_A\rho_B\nabla[\mu_B - \mu_A] + \eta \quad (7)$$

The distribution of the Gaussian noise η satisfies the fluctuation−dissipation theorem:

$$\langle\eta(\mathbf{r}, \mathbf{t})\rangle = 0 \quad (8)$$

$$\langle\eta(\mathbf{r}, \mathbf{t})\eta(\mathbf{r}', \mathbf{t}')\rangle = -\frac{2Mv}{\beta}\delta(t-t') \times \nabla_{\mathbf{r}}\cdot\delta(\mathbf{r}-\mathbf{r}')\rho_A\rho_B\nabla_{\mathbf{r}'} \quad (9)$$

where M is a bead mobility parameter. The kinetic coefficient $Mv\rho_A\rho_B$ models a local exchange mechanism. The Langevin equations are constructed for an incompressible system with dynamic constraint:

$$\rho_A(\mathbf{r}, t) + \rho_B(\mathbf{r}, t) = \frac{1}{v} \quad (10)$$

where v is the average bead volume.

2.2. Shear Behavior. For an incompressible block copolymer system, the dynamic equation for a fluctuating scalar field, $\phi_{\mathbf{k}}$, is analyzed using the Fokker−Planck equation[30]

$$\frac{\partial P}{\partial t}[\phi, t] = \int_k \frac{\delta}{\delta\phi_{\mathbf{k}}}\left[\mu\left(\frac{\delta}{\delta\phi_{-\mathbf{k}}} + \frac{\delta H[\phi]}{\delta\phi_{-\mathbf{k}}}\right) - A\omega\cos\omega t k_x\frac{\partial}{\partial k_y}\phi_{\mathbf{k}}\right]P[\phi, t] \quad (11)$$

and $\phi_{\mathbf{k}}$ is described by the Landau−Brazovskii Hamiltonian[31]

$$H[\phi] = \frac{1}{2}\int_k[\tau + (k-k_0)^2]\phi_{\mathbf{k}}\phi_{-\mathbf{k}} + \frac{1}{3!}\int_{k_1}\int_{k_2}\int_{k_3}\xi(\mathbf{k}_1, \mathbf{k}_2, \mathbf{k}_3, \mathbf{k}_4)\phi_{\mathbf{k}1}\phi_{\mathbf{k}2}\phi_{\mathbf{k}3} + \frac{1}{4!}\int_{k_1}\int_{k_2}\int_{k_3}\int_{k_4}\lambda(\mathbf{k}_1, \mathbf{k}_2, \mathbf{k}_3, \mathbf{k}_4)\phi_{\mathbf{k}1}\phi_{\mathbf{k}2}\phi_{\mathbf{k}3}\phi_{\mathbf{k}4} \quad (12)$$

where τ is a temperature-controlling parameter, k_0^{-1} is an intrinsic length scale of the block copolymer, μ is an Onsager coefficient that is approximated by $\mu = \mu(k_0)$ and assumed to be frequency independent.[32,33] The last term in eq 11 describes a coupling between the shear flow $\mathbf{v} = A\omega\cos\omega t y\mathbf{e}_x$ and the gradient of the $\phi_{\mathbf{k}}$. After some approximations,[32] Fredrickson has shown that the effective steady-state thermodynamical potential has the following form:

$$\Phi_{lam} = \Phi_{lam}^{(0)} + \beta\Phi_{lam}^{(1)}F(\dot\gamma)\cos(\theta), \quad F(\dot\gamma) = \begin{bmatrix}-\dot\gamma^2 & \dot\gamma \to 0 \\ \dot\gamma^{-1/3} & \dot\gamma \to \infty\end{bmatrix} \quad (13)$$

where $\dot\gamma$ denotes the shear rate, γ is the shear strain, the angle θ determines the orientation of the lamellae ($\theta = 0$ corresponds to the parallel lamellae), and Φ_{lam}^0 denotes the orientation-independent part of the potential Φ_{lam}. This equation predicts the parallel lamellae to be stable at low, and the perpendicular lamellae at high, shear rates.

Morozov and Fraaije[34] applied a similar formalism to the reorientational transitions occurring in the hexagonal phase. Analogizing to the eq 13, they got the following equation

$$\Phi_{hex} = \Phi_{hex}^{(0)} + \beta^3\Phi_{hex}^{(1)}F(\dot\gamma)\cos(6\theta) \quad (14)$$

where the angle θ determines the orientation of the hexagonal lattice ($\theta = 0$ corresponds to the orientation in real space). Generally, the potential Φ_{lam} or Φ_{hex} is time dependent. In this model, the minimum of Φ determines the stable orientation, and the potential Φ can be viewed as a dynamical extension of the equilibrium free energy. Using the equations above, the orientational phase diagram can be constructed.

2.3. Simulation Parameters. To specify the chemical nature of the system in a MesoDyn simulation, two sets of parameters must be defined: one is the chain topology in terms of repeat segments (or beads), and the other is the interaction energies of the various components. For the first set, MesoDyn uses a Gaussian chain "spring and beads" description, in which all segments are the same size and the chain topology depends on the coarsened degree of the original system. In this model, springs mimic the stretching behavior of a chain fragment and different kinds of beads corresponding to different components in the block copolymer. In this work, we selected the Pluronic polymer P65. Each bead in the Gaussian chain is a statistical unit, representing a number of "real" monomers. So the choice of the Gaussian chain should be an important aspect of the method. van Vlimmeren et al.[35] got a simple relationship between the atomistic chains and Gaussian chains for Pluronics:

$$\frac{X}{x} \approx 4.3, \qquad \frac{Y}{y} \approx 3.3 \tag{15}$$

where X and Y refer to the number of units for PEO and PPO monomers, which are 19 and 29 in P65 polymer, respectively. x and y are the numbers of coarsened chain topology. Thus, we can get $x \approx 4.4$ and $y \approx 8.8$, respectively. However, because both x and y have to be integers, the above equations cannot be solved exactly. Therefore, we choose the Gaussian chain of P65 as $A_4B_9A_4$, where the solvophobic B blocks represent PPO and the solvophilic A blocks are PEO. Moreover, one bead W represents water in the MesoDyn simulation. From our simulations in this paper, the Gaussian chain $A_4B_9A_4$ is reasonable for the simulated morphology with the experimental results.

The interaction energies ϵ_{IJ} [in eq 5] of the various types of segments in MesoDyn represents the pairwise interactions of beads, which are similar to that defined in the Flory−Huggins model.[36] It can be derived either from the atomistic simulation,[36,37] empirical methods,[38] or from experimental data such as vapor pressure data.[35] The simplest approach is based on regular solution theory and relates the Flory−Huggins parameter χ to the component solubility parameter δ. These parameters can be considered as the nonideal interactions that are included via a mean-field approach, and the strength of repulsion interaction between different components is characterized by $\epsilon_{AB} > 0$ in units of kJ/mol. The effective mean-field interactions vary with both concentration and temperature, $\chi = \alpha + \beta/T$. In these simple terms, α represents the entropic contribution, which is added to take into account the difference in the size of solvent and solute atoms, and β represents the enthalpic contributions.

In MesoDyn, the solvent−polymer interaction parameters are estimated as

$$\chi_{eff} = (\delta_I - \delta_J)^2 V_{ref}/RT + \chi_S \tag{16}$$

where V_{ref} is the reference volume (i.e., monomer volume). The entropy contribution to the mixing energy χ_S is neglected in this work because it is a relatively small correction in comparison to the other term.[39] The solubility parameter δ is related to each component's volumetric cohesive energy density E_{coh}/V of the system via the definition[39]

$$\delta = \sqrt{E_{coh}/V} \tag{17}$$

The values for δ may also be estimated for various polymers by empirical methods, e.g., Bicerano's methods,[40] or calculated directly from atomistic simulation [using eq 17].

In fact, the interaction parameters are also composition-dependent for Pluronics solution. Bae et al.[41] used an extended Flory−Huggins equation to investigate the relationship between the parameters and concentrations for vapor−liquid or liquid−liquid equilibria at different temperatures through the vapor pressure method and the semiempirical model. In MesoDyn, the pairwise interactions should be considered as the effective Flory−Huggins parameters, like Baulin and Halperin's work,[42] $\bar{\chi} = \chi_{eff} + f(\phi)$. On the basis of the solubility of polymer in water, when $\chi > 0.5$, the polymer is not easily dissolved in the solvent. However, from the successful simulations for the plurorics solution before,[24−28,35−36,43−45] χ_{AW} and χ_{BW} are selected as the values from 1.35 to 1.7 at different concentrations from the atomic simulations. Obviously, the parameters should be considered as the "effect" Flory−Huggins parameters χ_{eff}. We choose to focus on $\bar{\chi}$ because measurements of colligative properties, such as vapor pressure and osmotic pressure, yield $\bar{\chi}$ rather than χ_{eff}. Other two-state models[46−48] also showed the effect Flory−Huggins parameters for the water-soluble polymers. Some experiments and models[49] showed that there is a solubility gap for water−PEO solution in a low concentration at high temperature. In our simulation, we select the ternary block copolymer (PEO−PPO−PEO), and the concentration of spherical micelles formed for $A_4B_9A_4$ is more than 43 vol % through our simulation. We believe that these models are in fact suitable candidates for the description of aqueous solutions of neutral water-soluble polymers in general. The phase behavior of Pluronic solutions has been studied successfully by many authors using this model in the past decade, such as PL64, R25, and others.[24−28,35−36,43−45]

In our simulation, the effect Flory−Huggins parameters are chosen to be $\chi_{eff,\ AW} = 1.4$, $\chi_{eff,BW} = 1.7$ for solvent−polymer interactions and $\chi_{eff,AB} = 3.0$ for polymer−polymer interactions. These interaction parameters are the same as for aqueous Pluronic polymer surfactant solution, previously used in our[28,43] or other studies.[24−27,35−36] For all simulations, the dimensionless parameters in MesoDyn program have been chosen as (see details in refs 24, 35): the time step $\Delta\tau = 50$ ns (dimensionless time step $\Delta\tau = 0.5$), the noise scaling parameter $\Omega = 100$, the compressibility parameter $\kappa'_H = 25$, the grid parameter $d = ah^{-1}$ 1.1543, and the total simulation time is 50 000 steps (i.e., 2.5 ms). All the simulations are in a cubic grid with $32 \times 32 \times 32$ cells of mesh size h. The simulations are performed at 298 K. All the simulations are carried our using MesoDyn module in a commercial software package Cerius^2, version 4.6, from Accelrys, Inc.[50]

3. Results and Discussion

3.1. Phase Behaviors in the Absence of Shear. *3.1.1. Micellar Phase.* When the polymer concentration in water is higher than critical micelle concentration (cmc), micelles start to form. Different concentrations of Pluronics solutions, in which the spherical micelles formed, were found using MesoDyn simulations. For example, the 24 vol % $PEO_{26}PPO_{40}PEO_{26}$ ($A_6B_{12}A_6$) solution as spherical micelles was investigated by Lam,[36] while 50 vol % concentration $PEO_{13}PPO_{30}$ PEO_{13}-($A_3B_9A_3$) was selected by Altevogt.[27] These simulations show that the ratio of PPO and PEO can affect the concentrations in which the spherical micelles formed. In our simulation, the morphology of P65($A_4B_9A_4$) solution remains in spherical micelles even to fairly high concentration 43−45 vol % (see Figure 1).

In a 32 nm × 32 nm × 32 nm box, the numbers of spherical micelles are about 84−86 for 43−45 vol % systems. Then, the

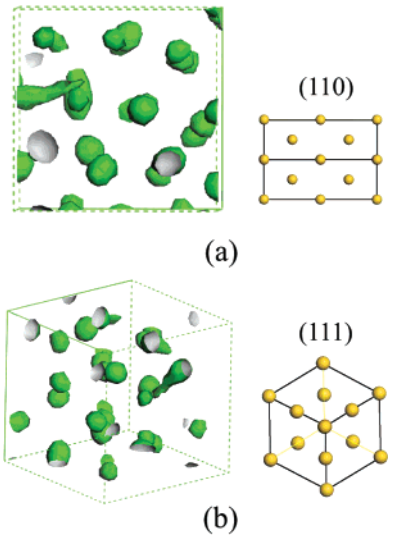

Figure 2. Three-dimensional autocorrelation micellar cube of 45 vol % obtained from reconstructing slices: (a) (110) plane; (b) (111) plane. To clearly show the (110) and (111) structures, the normal fcc structures for different planes are shown in the right.

average core radius, R_c, of PO monomer is calculated, which is about $R_c \approx 30$ Å. To a good approximation, the aggregation number (N) scales linearly with the third power of the core radius, R_c:[51]

$$NnV_{PO} = \frac{4}{3}\pi R_c^3 \tag{18}$$

where $n = 29$ is the PO degree of polymerization, and the propylene oxide volume is $V_{PO} = 95.4$ Å^3. This leads to an aggregation number of $N \approx 41$ for spherical micelles in the range of concentrations. de Bruijn[52] calculated $N = 23$ for P65 solution by a numerical self-consistent-field model. In fact, even if the same technique was used, the different aggregation numbers for the same Pluronics were still reported. For example, the aggregation numbers of Pluronic L64 are 88 at 315.5 K,[53] 13 at 315 K, and 50 at 318 K[54] by different groups using the same light scattering experiments. Our calculation is another reference aggregation number for P65 at 298 K.

In the micellar cubic phase, although the detailed structures are not yet established, presumably all of these structures are based on packing of discrete micellar aggregates. Certain surfactant systems, such as the polyoxyethylene surfactant, can adopt as many as three distinct cubic phase structures in the region of the phase diagram that is adjacent to the micellar solution.[55] In MesoDyn, the 3D autocorrelation can describe the probability of finding another micelle at a certain distance and direction from a reference micelle.[36] After the 3D autocorrelation micellar cubic phase in a 22.4 nm × 22.4 nm × 22.4 nm box is reconstructed (Figure 2), there are a sufficient number of micelles to determine the ordering in 3D cubic micellar phase. The micellar phase is similar to the fcc (face-centered cubic) structure. If we look down the (110) and (111) planes in Figure 2a and b, the most obvious fcc structure can be found. There is a squashed hexagonal packing in the (110) plane and a regular hexagonal packing in the (111) plane, and both packings are indicative of a fcc lattice arrangement for the micellar phase.

In different Pluronic systems, the micellar phase can form bcc or fcc structure. Eiser and co-workers[56] found that the micelles of the polymer F108 ($PEO_{127}PPO_{48}PEO_{127}$) organize themselves into fcc symmetry, and F68 ($PEO_{76}PPO_{29}PEO_{76}$) system leads to a bcc symmetry. The fcc structures have a higher packing ratio of 0.744 than bcc (0.68). As a more efficient packing order, the fcc arrangement is adopted by the system to pack a large number of micelles. In our simulation, there is no bcc micellar phase for P65. We think that the short-range intermicellar interaction prefers fcc micellar structure. Moreover, the short repulsive interactions between micelles will be destroyed as the numbers of micelles increases. So, the associated spherical micelles, i.e., wormlike micelles, will form with the increase of concentration.

In our simulation, the wormlike micelles can be found in the range of 46−56 vol % concentration. In this stage, the spherical micelles start to coalesce and then form wormlike micelles. This change can be manifested by a shift in size toward long aggregates, as shown in Figure 3. The wormlike micellar growth has been observed over time, and it shows that the wormlike micelles grow individually by chain transfer as well as by coalescence with spherical micelles one by one.

3.1.2. Bicontinuous and Lamellar Phases. In the range of concentration 57−89 vol %, both PO- and EO-rich domains

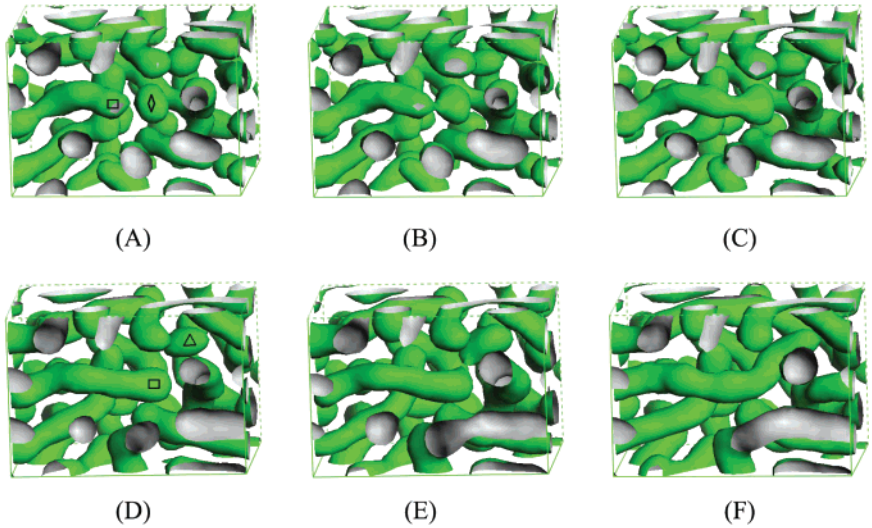

Figure 3. Wormlike micelles of various sizes are formed due to random association with neighboring chains in 50 vol % system. Coalescence of wormlike micelle and spherical micelle with increasing time steps: (A) 35 μs, (B) 40 μs, (C) 50 μs, (D) 125 μs, (E) 140 μs, (F) 250 μs. Note: □ wormlike micelle; ◇, △ spherical micelles that coalesce.

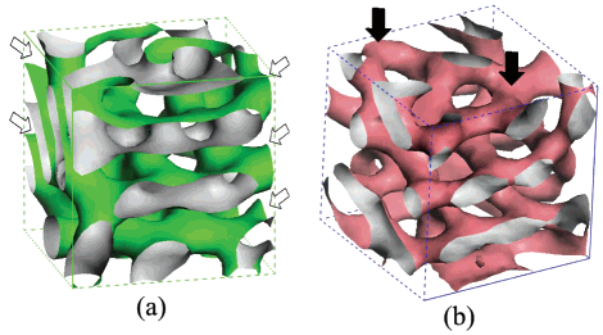

Figure 4. Enlarged small parts of snapshots (24 nm × 24 nm × 24 nm) at 70 vol % concentration from Figure 1a: (a) PO isosurfaces; (b) water isosurfaces, which water molecules mainly lie in EO rich domains. The empty arrow points out the lamellar structures in the bicontinuous phases, and the black arrow points out the joints of two lamellar structures.

can coagulate into one percolating cluster according to the cluster analysis in MesoDyn. Therefore, this phase in these concentrations is bicontinuous. Because there are too many defects, it is difficult to deduce the type of bicontinuous phase from 3D concentration fields of PO or EO in the simulation box. In Figure 4a, we notice that many lamellar structures are still found in the bicontinuous phases of PO isodensity profiles (the white arrow in Figure 4a), and the enlarged view of domain morphology from the profiles of water fields clearly indicates the joints between different bicontinuous lamellas (the black arrow in Figure 4b). Therefore, we think that the type of bicontinuous phase is gyroid, and the gyroid-type phase is still without global symmetry throughout the sample. In our simulation, the system can remain in this phase for a very long time and the gyroid-type structure rearranges slowly with time evolution (see the changes of order parameters of 70 vol % in Figure 6b).

At 89.5 vol % concentration, through the isodensity profile of PO, the lamellar phase is found (in Figure 1). Herein, we focus on the change of morphology around this concentration. We noticed that the isodensity profile of water is a little orderless below the lamellar concentration (89 vol % in Figure 5a), however some original lamellar morphologies of water are still observed at both sides of box. In the typical lamellar phase (89.5 vol %), some coalesced points between two lamellas are arresting. More coalesced joints would be found among different lamellas at above the lamellar concentration, and at last they form a whole netlike structure (90 vol % in Figure 5c). In brief, water molecules must move along different channels in the bicontinuous phase (i.e., the concentration is below 89.5 vol %), while they can move cross the netlike structures when the concentrations are above the lamellar concentration (89.5 vol %). Most published investigations have paid more attention to the morphology of hydrophobic PO blocks. However, according to our above investigations, we believe that the special water channels in bicontinuous or lamellar phases could have more special functions. For example, it offers some channels in drug delivery, and the drug can be delivered through the different water channels in the same bicontinuous or lamellar phases. Because the special netlike structures of water are formed above the concentration 89.5 vol %, we define the defected

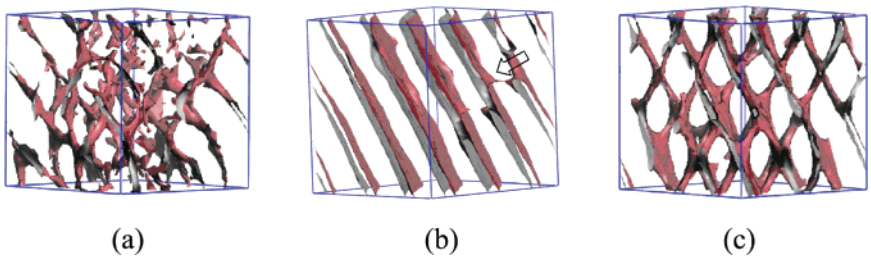

Figure 5. Isodensity profile of water around lamellar phase systems: (a) 89 vol %; (b) 89.5 vol %; (c) 90 vol %. The empty arrow in Figure 5b points out the coalesced points between two lamellas.

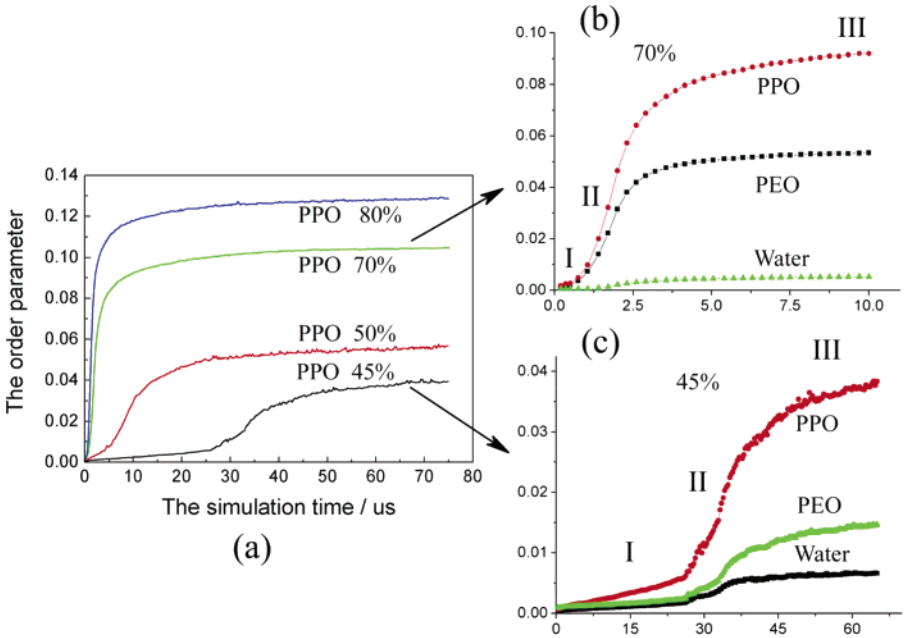

Figure 6. Order parameter plot with time evolution for different systems. The inset shows the exploded view of the nucleation stage.

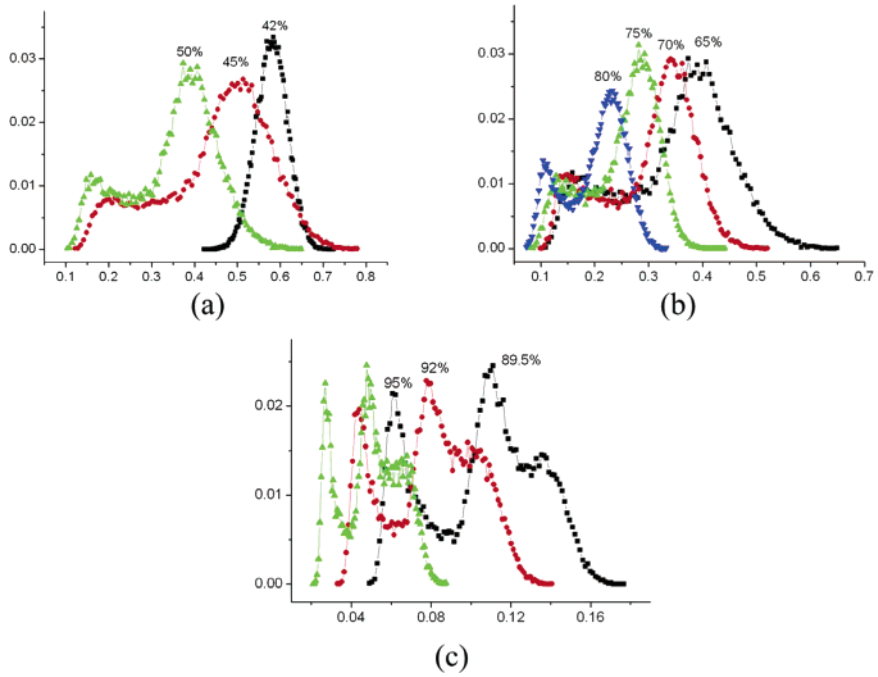

Figure 7. Structure factors of P65 solutions. Each graph is obtained by performing a 3D Fourier transform and subsequent averaging over all directions: (a) premicellar (42 vol %), spherical micellar (45 vol %) and wormlike micellar phase (50 vol %); (b) bicontinuous phase (65, 70, 75, and 80 vol %); (c) lamellar phase (89.5 vol %) and defected lamellar phase (92 and 95 vol %). Units on the horizontal axis are h^{-1}; units on the vertical axis are arbitrary (but the same for all systems.).

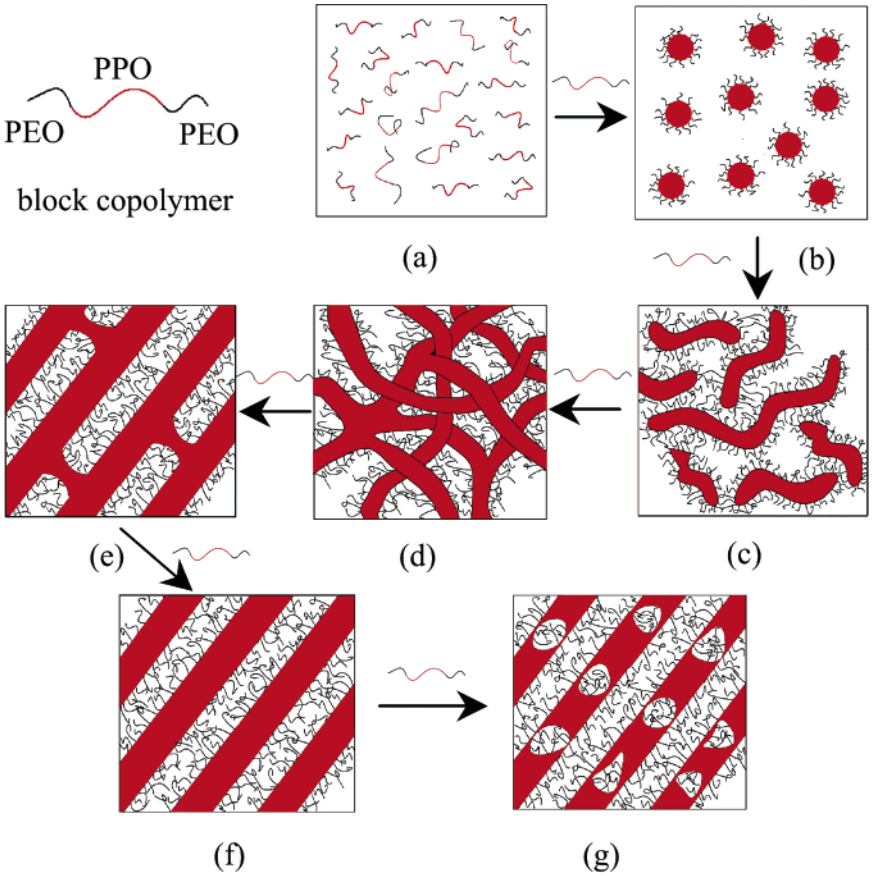

Figure 8. Schematic representation of spherical micelles, wormlike micelle, bicontinuous, and lamellar phases of PEO−PPO−PEO types of block copolymers with the increase of concentration: (a) monomer in the solution, (b) spherical micelle consisting of many copolymer molecules; (c) wormlike micelle; (d) bicontinuous phase; (e) lamellar phase with some joints between two lamellas; (e) lamellar phase; (f) defected lamellar phase with some EO cores in PO lamellas.

lamellar phase (L1 in Figure 1) in order to distinguish it from the typical lamellar phase.

3.1.3. The Structure Analysis. The order parameter, P, represents the characteristics of phase separation. It is

defined as

$$P \equiv \overline{\theta - \bar{\theta}^2} = \frac{\int_V \sum_I [\theta_I^2(r) - (\theta_I^0)^2]\, dr}{V} \qquad (19)$$

where θ is the polymer volume fraction and V is the volume of cells. P is the mean-squared deviation from homogeneity in the system, which captures both the effects of phase separation and compressibility.

The time evolution of the order parameters is shown in Figure 6, and the phase separation is faster in high concentration. This is not surprising because the thermodynamic driving forces for phase separation in high concentrations are larger. As an example of 45 vol % solution (Figure 6c), we can observe that the time evolution of the phase in three stages. At first (I in Figure 6c), premicelles are formed, which correspond to the nucleation of several polymer aggregates, and the order parameter changes slowly. In this stage, the morphology of the system varied little. Then, micelles start to form, and the order parameter ascends rapidly (II in Figure 6c). In this second stage, the system forms quickly the raw morphologies of micelles. This process is about tens of μs. Finally, the system changed in a slow way to overcome the defects formed in the previous stage, which is time-consuming (III in Figure 6c). For other systems, in which bicontinuous or lamellar phases form, the order of parameters also show that these systems go through a similar process (like the 70 vol % solution in Figure 6b), and the difference between them is only the time-consuming phase separation. Specially in the first stage I, the process forming the original prestructures in vol 70% system (Figure 6b) is much shorter than that in a 45 vol % system (Figure 6c). This indicates that the concentration of polymer influences not only the occurrence of different morphologies but also the formation rate of different phases.

Detailed analysis of the structure factors (Figure 7) shows that diffraction peaks of water are located at different frequencies with different phases. At the micelle phases, only one diffraction peak for a per-micelle system is found at the high frequency 1.5−2.2 q_0 (42 vol % in Figure 7a). It indicates the weak ordering, but with increasing the concentration of P65, the second diffraction peaks are formed at the low frequency around 5.8 q_0 for the spherical and wormlike micelle systems (45, 50 vol % in Figure 7a).

At the bicontinuous phases (Figure 7b), the intensity of the second peak increases with the increasing of the concentration, and the difference of two frequencies, $\Delta q = q_1 - q_2$, decreases. It occurs because that the two water channels are gradually close.

In the lamellar phases (Figure 7c), the height of the first and second peak are almost the same, and this indicates that the water properties in different channels are similar. Besides, a third peak forms around the first frequency; it shows that water in the netlike structures (Figure 5c) is different from that in the lamellas. Van Vlimmeren[35] has also seen the three peaks for L64 in the lamellar phases. We think the third peak represents the boundary region connecting the different lamellar microdomains.

In brief, with increasing of the concentration of P65, different phases, such as spherical micelle, wormlike micelle, bicontinuous, and lamellar phases, are formed in aqueous solution. Figure 8 shows schematic representation of these phases with increasing of the concentration. In spherical micelles (Figure 8b), the hydrophobic blocks PO are gathered into a spherical core and the hydrophilic blocks EO are solvated by water, then wormlike micelles are formed due to the coalescent of spherical micelles (Figure 8c), and there are two different water channels in the bicontinuous phase (Figure 8d); at last, the lamellar phases that have many joints between two lamellas (Figure 8f), and the defected lamellar phases that some EO cores are in PO lamellas, are formed in the high concentration (Figure 8g).

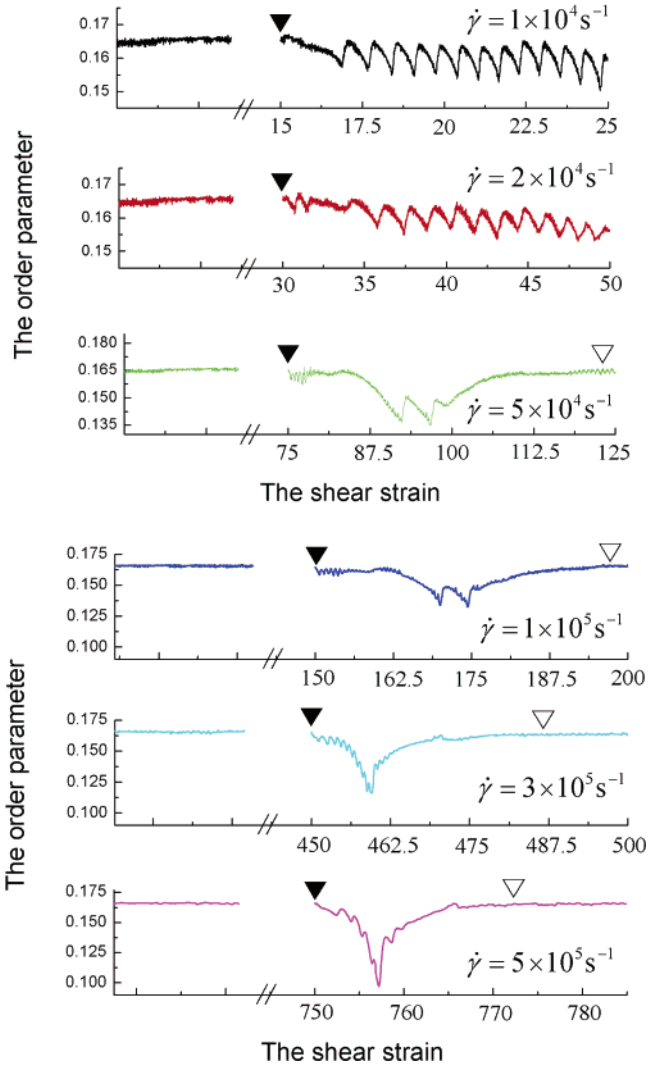

Figure 9. Order parameter with the increase of shear strain on the morphology for 89.5 vol % system, which has been formed during simulation time 1.5 ms. Note: ▼ points to the time that the shear is applied (1.5 ms), and □ points to the time that the new morphology has been formed. In the simulations, the time of new morphologies formed under different shears are 0.9 ms ($\dot{\gamma} = 5 \times 10^4\ s^{-1}$), 0.46 ms ($\dot{\gamma} = 1 \times 10^5\ s^{-1}$), 0.1 ms ($\dot{\gamma} = 3 \times 10^5\ s^{-1}$), and 0.04 ms ($\dot{\gamma} = 5 \times 10^5\ s^{-1}$), respectively.

3.2. Phase Behaviors in the Presence of Shear. In this section, the effect of shear to different phases, micelle, bicontinuous gyroid, and lamellar phase in different systems, is investigated. The shear-induced transitions between these phases are observed. In these simulations, the time evolution of the density field under simple steady shear flow, $v_x = \dot{\gamma}y$, $v_y = v_z = 0$, can be described by a time-dependent Landau−Ginzburg type equation with a convective term and a stochastic term.[57−59] The shear rate $\dot{\gamma}$ allows us to apply results to different systems. For example, for a typical diffusion coefficient $10^{-14} - 10^{-13}$ $m^2\ s^{-1}$, the shear rate is $D/\dot{\gamma} \sim 10 - 10^2\ s^{-1}$.[60] In our simulations, the weakest shear applied is $\dot{\gamma} = 1 \times 10^4\ s^{-1}$. From the diffusion coefficient D, one can extract a length scale $\lambda = \sqrt{D/\dot{\gamma}} \sim 1$ nm. This is comparable to the size of the micelles

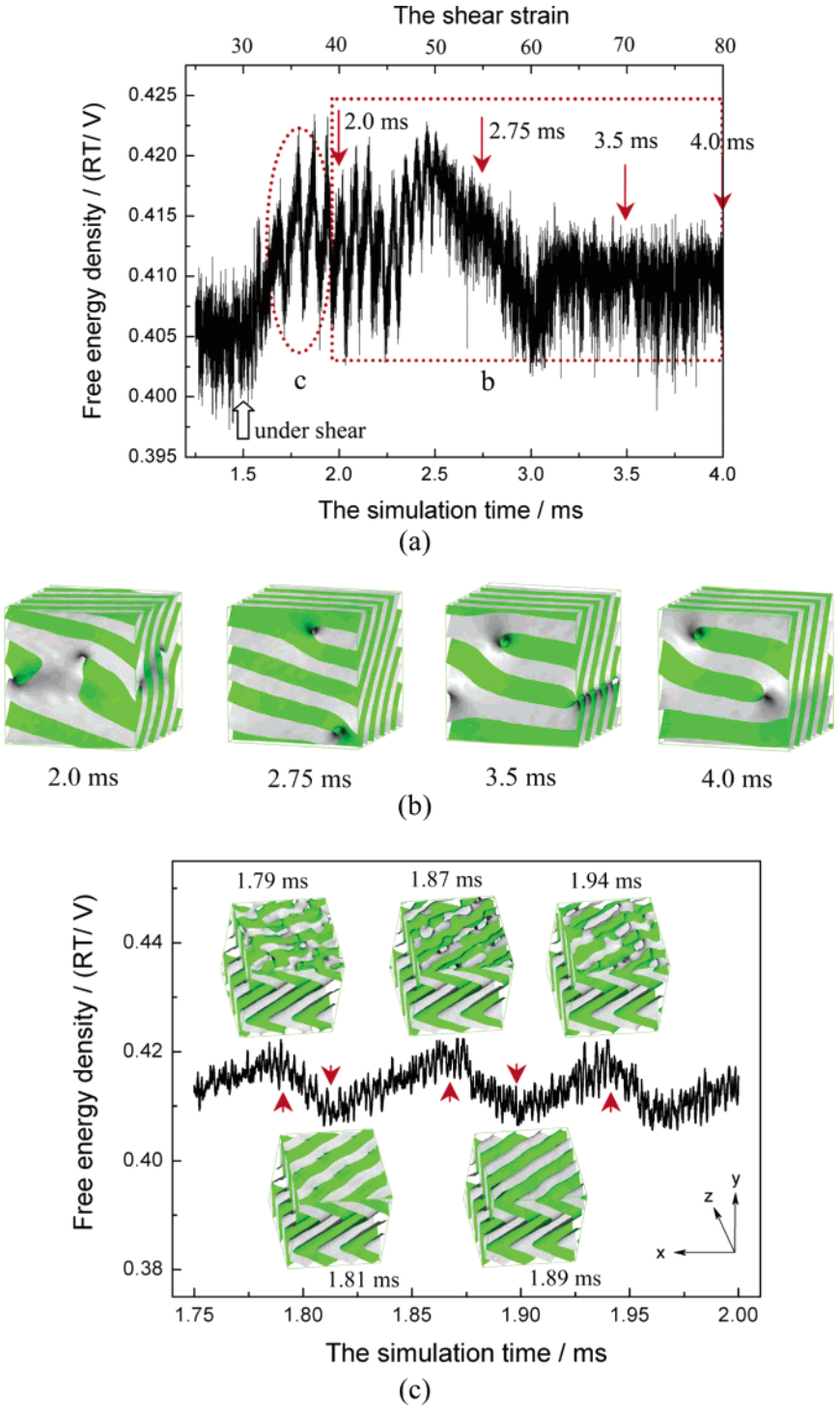

Figure 10. Free energy with time evolution and the shear strain for 89.5 vol % system ($\dot{\gamma} = 1 \times 10^4$ s^{-1}).

or the lamellar repeat spacing. Because the rate of perturbation by the shear exceeds the rate at which the structure can relax by diffusion, i.e., the length scales > ~1 nm, thus it is not surprising that the shear should be a perturbation of the phase behavior. In the following, two types of shears are applied. One is applied to the morphologies which have been formed after a long simulation in the absence of shear; the other is applied to the systems which are homogeneous density distributions at the beginning of simulation.

3.2.1. Effect of Shear to the Morphology Which Has Been Formed. To investigate the effect of shear on the morphology, the first type of shear is applied to the typical lamellae, which has been formed at 30 000 steps (1.5 ms) for 89.5 vol % system in the presence of shear. If different shears are applied to the system after 1.5 ms, the morphology starts to deform, and the order parameter which gives information about the ordered structures also changes (Figure 9).

Under weak shear $\dot{\gamma} = 1 \times 10^4$ s^{-1} or $\dot{\gamma} = 2 \times 10^4$ s^{-1}, the order parameter oscillates with the increase of shear strain (Figure 9a). The morphologies are shown in Figure 10c at one periodical variation of the free energy density at $\dot{\gamma} = 1 \times 10^4$ s^{-1}. In Figure 10c, we notice that the morphologies in the high peak of free energy density at 1.79, 1.87, and 1.94 ms are similar, which are different with those at the bottom of free energy density at 1.81 and 1.89 ms. These phenomena mean that the morphology can be restored under weak shear. However,

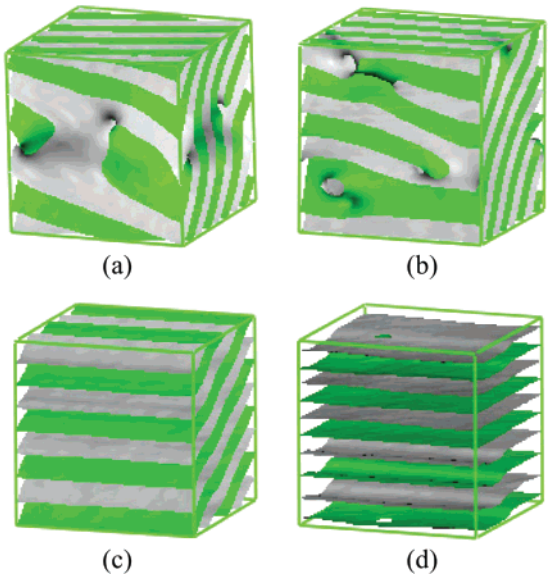

Figure 11. Results of shear in the *x* direction under different strong shears at the simulation 0.5 ms. (a) $\dot{\gamma} = 1 \times 10^4\ s^{-1}$, (b) $\dot{\gamma} = 2 \times 10^4\ s^{-1}$, (c) $\dot{\gamma} = 3 \times 10^5\ s^{-1}$, (d) $\dot{\gamma} = 5 \times 10^5\ s^{-1}$.

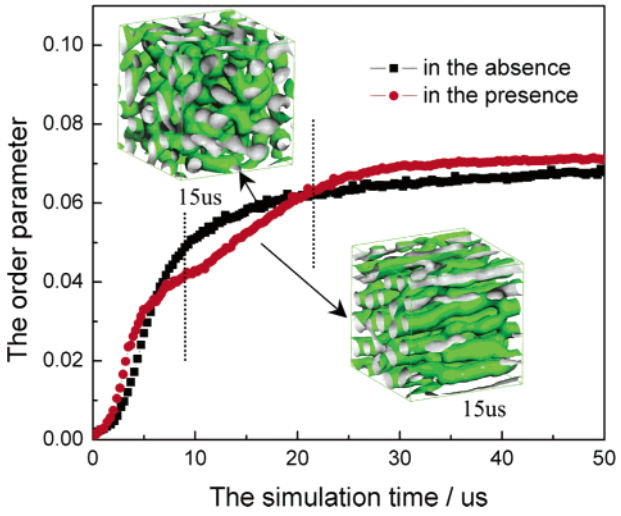

Figure 12. Order parameters in the absence and presence of shear ($\dot{\gamma} = 5 \times 10^5\ s^{-1}$). Two isodensity profiles of PO are shown at 15 μs.

the order parameters under strong shear get steady values after short oscillation, and the new morphology is formed in a short time (in Figure 9, when $\dot{\gamma} > 2 \times 10^4\ s^{-1}$). We notice that the time of new morphology formed is shorter with the stronger shears; there are 0.9, 0.46, 0.1, and 0.04 ms for $\dot{\gamma} = 5 \times 10^4\ s^{-1}$, $\dot{\gamma} = 1 \times 10^5\ s^{-1}$, $\dot{\gamma} = 3 \times 10^5\ s^{-1}$, and $\dot{\gamma} = 5 \times 10^5\ s^{-1}$, respectively. The shear $\dot{\gamma} = 5 \times 10^5\ s^{-1}$ can give the order morphology in the shortest simulation time. Therefore, the strength of shear is set as $\dot{\gamma} = 5 \times 10^5\ s^{-1}$ to investigate its effect on the morphology of Pluronic solution.

Different strong shears (from $\dot{\gamma} = 1 \times 10^4\ s^{-1}$ to $\dot{\gamma} = 5 \times 10^5\ s^{-1}$) lead to the similar morphology with little of defects (holes in lamellae) in 89.5 vol % solution, as shown in Figure 11. Under weak shears, the small tilt of the whole picture indicates that the alignment to the flow direction is not yet completely perfect ($\dot{\gamma} = 1 \times 10^4\ s^{-1}$ and $\dot{\gamma} = 2 \times 10^4\ s^{-1}$, Figure 11a and b), while the strong shear very quickly breaks up the remaining connections, and a few holes in the lamellae quickly diminish with time evolution ($\dot{\gamma} = 3 \times 10^5\ s^{-1}$ and $\dot{\gamma} = 5 \times 10^5\ s^{-1}$, Figure 11c and d). It is known that the morphology with little defects may be viewed when the systems are in nonequilibrium in a short simulation time. To get the reason whether the defect in the morphology is the result of weak shear or nonequilibrium, another long simulation is run for the weak shear $\dot{\gamma} = 2 \times 10^4\ s^{-1}$, and the changes of free energy density are also shown with time evolution in Figure 10. We notice that the free energy density of simulation system under weak shear can get equilibrium at a long time (3.0 ms); however, the morphologies with little defects are still shown during the simulation (Figure 10b). Apparently, the defects in the morphology are the result of weak shear, and the morphology will keep the defects under weak shear strain for a long time. However, the strong shears can eliminate the defect. At the end of simulation, the direction of lamellae is parallel to the flow direction in short time (Figure 11d).

3.2.2. Effect of Shear to the Homogeneous System. The system 55 vol % is selected as an example to investigate the phase separation under shear, and the phase morphology of 55% solution is a wormlike micelle in the absence of shear (Figure 1a). After applying shear ($\dot{\gamma} = 5 \times 10^5\ s^{-1}$) to the homogeneous system, the morphology slowly deforms. The order parameter with time evolution shows the trend (Figure 12). At the beginning of simulation, the order parameters increase rapidly, and the value in the presence of shear is more than that in the

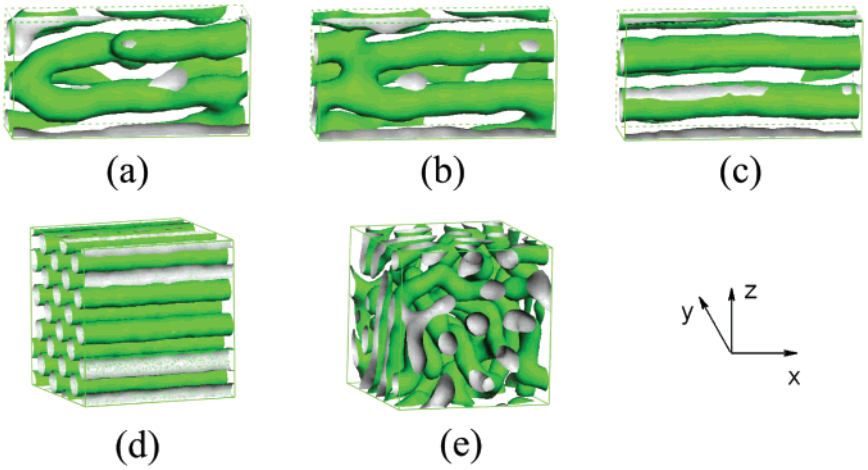

Figure 13. Hexagonal phase are formed under shear ($\dot{\gamma} = 5 \times 10^5\ s^{-1}$) in contrast with the wormlike micelles in equilibrium 55 vol % system. Wormlike micelles under shear coalesce with the increasing time steps: (a) 70 μs, (b) 85 μs, (c) 90 μs, (d) 1 ms, (e) 2.5 ms (the morphology in the absence of shear). Note: in order to clearly show the change of morphology, (a−c) are 32 nm × 16 nm × 16 nm box, (g) and (h) are 32 nm × 32 nm × 32 nm box.

absence of shear before the micelles start to form in the first 5 μs (<100 steps). It means that the block polymers are easily aggregated when the external force is applied. Then, with the increase of the simulation time, the main special structure of wormlike micelles hardly change in the presence or absence of shear, and the only difference between them is the direction of wormlike micelle. The shear-induced wormlike micelles parallel to the *x*-axis with a bigger order parameter from 50 to 20 μs (Figure 12) and the wormlike micelles in the absence of shear have random directions. After the simulation is more than 22.5 μs (450 steps), the original hexagonal structures paralleling the *x*-axis are formed; at that time, the order parameter under shear is bigger. Figure 13 shows the coalescence of wormlike micelle under shear with time evolution. When the shear continues to the system, the separate pieces of wormlike micelles start to coalesce and form pattern aligned in the flow direction (Figure 13a−c). New structures consisting of hexagonally packed cylindrical clusters are formed at the end of simulation, as shown in Figure 13d.

In fact, the phase diagram of P65 in the solution has been investigated by Hoffmann et al.[61] through the macroscopic phases checked for birefringence 10 years ago. They found P65 solution could form from an isotropic, hexagonal to lamellar phase in all the concentrations at 298 K. As a coarse glance, our simulated morphologies in the absence of shear are different from their experimental results, while the morphologies under shear are similar to their results. We notice that they used the birefringence method to investigate the macroscopic phase, and the Pluronics solutions were first placed into a vibrator until clear phases were obtained, and then the solutions were put in a temperature bath and left to equilibrate. The dissolution of P65 in a vibrator in their experiments indicates that some external forces should be added and rapid the dissolution of Pluronics in the solution, we think that the external force likes the shear strain in our simulation under shear. Thus, it is reasonable for our simulations that the morphologies under shear are similar to their experimental results.

Summary

The phase behaviors of P65 solution are simulated using the MesoDyn method in the presence and absence of shear. The influence of concentration and shear on the phase separation with time evolution is discussed.

In the absence of shear, there are three morphologies formed in aqueous solution. The first is a spherical micelle, which has hexagonal packing and a fcc (face centered cubic) micellar structure and wormlike micelle, the second is the bicontinuous phase, which belongs to a gyroid-type connectivity, and the third is the lamellar phase. Under shear, only two morphologies, i.e., hexagonal and lamellar phases which align in the flow direction, are formed in all concentrations. We notice that the order parameters oscillate under the weak shears, while they go to the steady values under strong shear after shorter oscillation, and the morphologies of systems have similar changes under different strong shears. In conclusion, mesoscopic simulation can be considered as an adjunct method for the description of mesoscale morphology formation and can give mesoscale information for the experiments.

Acknowledgment. This work was supported by the National Natural Science Foundation of China (no. 20303011, 20573067).

References and Notes

(1) Alexandridis, P.; Holzwarth, J. F. *Langmuir* **1997**, *13*, 6074.
(2) Michels, B.; Waton, G.; Zana, R. *Colloids Surf., A* **2001**, *55*, 183.
(3) Patterson, I.; Chowdhry, B.; Leharne, S. *Colloids Surf., A* **1996**, *111*, 263.
(4) Pedersen, J. K.; Svaneborg, C. *Curr. Opin. Colloid Interface Sci.* **2002**, *7*, 158.
(5) King, S. M.; Heenan, R. K.; Cloke, V. M.; Washington, C. *Macromolecules* **1997**, *30*, 6215.
(6) Eiser, E.; Molino, F.; Porte, G.; Diat, O. *Phys. Rev. E* **2000**, *61*, 6759.
(7) Liu, Y.; Chen, S.-H.; Huang, J. S. *Macromolecules* **1998**, *31*, 2236.
(8) Liu, Y.; Chen, S.-H.; Huang, J. S. *Macromolecules* **1998**, *31*, 6226.
(9) Jørgensen, E. B.; Hvidt, S.; Brown, W.; Schillén, K. *Macromolecules* **1997**, *30*, 2355.
(10) Chen, S. H.; Mallamace, F.; Faraone, A.; Gambadauro, P.; Lombardo, D.; Chen, W. R. *Eur. Phys. J., E* **2002**, *9*, 283.
(11) Liu, Y.; Chen, S.-H.; Huang, J. S. *Phys. Rev. E* **1996**, *54*, 1698.
(12) Chen, Z. R.; Issaina, A. M.; Kornfield, J. A.; Smith, S. D.; Grothaus, J. T.; Satkowski, M. M. *Macromolecules* **1997**, *30*, 7096.
(13) Schmidt, G.; Richtering, W.; Lindner, P.; Alexandridis, P. *Macromolecules* **1998**, *31*, 2293.
(14) Waton, G.; Michels, B.; Steyer, A.; Schosseler, F. *Macromolecules* **2004**, *37*, 2313.
(15) Groot, R. D.; Madden, T. J. *J. Chem. Phys.* **1998**, *108*, 8713.
(16) Hoogerbrugge, P. J.; Koelman, J. M. V. A. *Europhys. Lett.* **1992**, *19*, 155.
(17) Espanol, P.; Warren, P. *Europhys. Lett.* **1995**, *30*, 191.
(18) Groot, R. D.; Warren, P. B. *J. Chem. Phys.* **1997**, *107*, 4423.
(19) Fraaije, J. G. E. M. *J. Chem. Phys.* **1993**, *99*, 9202
(20) Maurits, N. M.; Altevogt, P.; Evers, O. A.; Fraaije, J. G. E. M. *Comput. Theor. Polym. Sci.* **1996**, *6*, 1.
(21) Maurits, N. M.; van Vlimmeren, B. A. C.; Fraaije, J. G. E. M. *Phys. Rev. E* **1997**, *56*, 816.
(22) Warren, P. B. *Curr. Opin. Colloid Interface Sci.* **1998**, *3*, 620.
(23) Jawalkar, S. S.; Adoor, S. G.; Sairam, M.; Nadagouda, M. N.; Aminabhavi, T. M. *J. Phys. Chem. B* **2005**, *109*, 15611.
(24) Fraaije, J. G. E. M.; van Vlimmeren, B. A. C.; Maurits, N. M.; Postma, M.; Evers, O. A.; Hoffman, C.; Altevogt, P.; Goldbeck-Wood, G. *J. Chem. Phys.* **1997**, *106*, 4260.
(25) Fraaije, J. G. E. M.; Sevink, G. J. A. *Macromolecules* **2003**, *36*, 7891.
(26) Lyakhova, K. S.; Zvelindovsky, A. V.; Sevink, G. J. A.; Fraaije, J. G. E. M. *J. Chem. Phys.* **2003**, *118*, 8456
(27) Altevogt, P.; Evers, O. A.; Fraaije, J. G. E. M.; Maurits, N. M.; van Vlimmeren, B. A. C. *J. Mol. Struct. (THEOCHEM)* **1999**, *463*, 139.
(28) Li, Y. M.; Xu, G. Y.; Chen, A. M.; Yuan, S. L.; Cao, X. R. *J. Phys. Chem. B* **2005**, *109*, 22290.
(29) Bai G. Y.; Nichifor, M.; Lopes, A,; Bastos, M. *J. Phys. Chem. B* **2005**, *109*, 518.
(30) Fredrickson, G. H. *J. Rheol.* **1994**, *38*, 1045.
(31) Fredrickson, G. H.; Helfand, E. *J. Chem. Phys.* **1987**, *87*, 697.
(32) Fredrickson, G. H. *J. Chem. Phys.* **1986**, *85*, 5306.
(33) Morozov, A. N.; Fraaije, J. G. E. M. *Phys. Rev. E* **2002**, *65*, 031803.
(34) Morozov, A. N.; Fraaije, J. G. E. M. *Phys. Rev. E* **2000**, *61*, 4125.
(35) van Vlimmeren, B. A. C.; Maurits, N. M.; Zvelindovsky, A. V.; Sevink, G. J. A.; Fraaije, J. G. E. M. *Macromolecules* **1999**, *32*, 646.
(36) Lam, Y. M.; Goldbeck-Wook, G. *Polymer* **2003** *44*, 3593−3605
(37) Zhang, M.; Choi, P.; Sundararaj, U. *Polymer* **2003**, *44*, 1979.
(38) Honeycutt, J. D. *Comput. Theor. Polym. Sci.* **1998**, *8*, 1.
(39) Wesoctt, J. T.; Qi, Y.; Capehart, T. W. *J. Chem. Phys.* **2006**, *124*, 134702.
(40) Bicerano, J. *Prediction of Polymer Properties*, 3rd ed.; Marcel Dekker: New York, 2002.
(41) Bae, Y. C.; Shim, J. J.; Soane, D. S.; Prausnitz, J. M. *J. Appl. Polym. Sci.* **1993**, *47*, 1193.
(42) Baulin, V. A.; Halperin, A. *Macromolecules* **2002**, *35*, 6432.
(43) Yuan, S. L.; Zhang, X. Q.; Xu, G.. Y.; Zhang, D. J. *J. Mol. Model.* **2006**, *12*, 406.
(44) Horvat, A.; Lyakhova, K. S.; Sevink, G. J. A.; Zvelindovsky, A. V.; Magerle, R. *J. Chem. Phys.* **2004**, *120*, 1117.
(45) Guo, S. L.; Hou, T. J.; Xu, X. J. *J. Phys. Chem. B* **2002**, *106*, 11397.
(46) Karlstrom, G. *J. Phys. Chem.* **1985**, *89*, 4962.
(47) Matsuyama, A.; Tanaka, F. *Phys. Rev. Lett.* **1990**, *65*, 341.
(48) Bekiranov, S.; Bruinsma, R.; Pincus, P. *Phys. Rev. E* **1997**, *55*, 577.
(49) Karlström, G. *J. Phys. Chem.* **1985**, *89*, 4962.
(50) One Molecular Simulation Software, Inc., see https://www.accelrys.com.
(51) Mortensen, K.; Pedersen, J. S. *Macromolecules* **1993**, *26*, 805.
(52) de Bruijn, V. G.; van den Broeke, L. J. P.; Leermakers, F. A. M.; Keurentjes, J. T. F. *Langmuir* **2002**, *18*, 10467.
(53) Zhou, Z.; Chu, B. *J. Colloid Interface Sci.* **1988**, *126*, 171.

(54) Almgren, M.; Bahadur, P.; Jansson, M.; Li, P.; Brown, W.; Bahadur. A. *J. Colloid Interface Sci.* **1992**, *151*, 157.
(55) Seddon, J. M.; Templer, R. H. *Philos. Trans. R. Soc. London A* **1993**, *344*, 377.
(56) Eiser, E.; Molino, F.; Porte, G.; Pithon, X. *Rheol. Acta* **2000**, *39*, 201.
(57) Kodama, H.; Doi, M. *Macromolecules* **1996**, *29*, 2652.
(58) Zvelindovsky, A. V.; van Vlimmeren, B. A. C.; Sevink, G. J. A.; Maurits, N. M.; Fraaije, J. G. E. M. *J. Chem. Phys.* **1998**, *109*, 8751.
(59) Zvelindovsky, A. V.; Sevink, G. J. A.; Fraaije, J. G. E. M. *Phys. Rev. E* **2000**, *62*, 3063.
(60) Zvelindovsky, A. V.; Sevink, G. J. A.; van Vlimmeren, B. A. C.; Maurits, N. M.; Fraaije, J. G. E. M. *Phys. Rev. E* **1998**, *57*, 4879.
(61) Wanka, G.; Hoffmann, H.; Ulbricht, W. *Macromolecules* **1994**, *27*, 4145.

MA061201B